

Tuning the nitrogen content and surface properties of nitrogen-doped carbon nanotubes synthesized using a nitrogen-containing ferrocenyl derivative and ethylbenzoate

Lucy M. Ombaka · Patrick G. Ndungu · Vincent O. Nyamori

Received: 23 June 2014 / Accepted: 16 October 2014 / Published online: 28 October 2014
© Springer Science+Business Media New York 2014

Abstract Aligned nitrogen-doped carbon nanotubes (N-CNTs) containing 6.4–15.7 wt% of nitrogen were synthesized by pyrolysis of 3-ferrocenyl-2-(4-cyanophenyl)acrylonitrile as the catalyst in either acetonitrile or a solution of acetonitrile and ethylbenzoate. For comparison, N-CNTs were synthesized by pyrolysis of 3-ferrocenyl-2-(4-cyanophenyl)acrylonitrile in toluene. The effect of oxygen and the carbon source used during synthesis was investigated. The use of 3-ferrocenyl-2-(4-cyanophenyl)acrylonitrile in acetonitrile as a nitrogen and carbon source selectively yielded mainly N-CNTs, while use of toluene as a carbon source yielded both N-CNTs and carbon spheres. Elemental analysis of the N-CNTs synthesized using both acetonitrile and ethylbenzoate (source of oxygen) indicated that addition of oxygen enhanced the nitrogen content of N-CNTs. This was further supported by results from Raman spectroscopy, X-ray diffraction (XRD), Fourier transform infrared spectroscopy and inverse gas chromatography surface energy analysis. The higher nitrogen-containing N-CNTs were less graphitic and showed a higher base constant (K_b) compared to N-CNTs synthesized without oxygen. Analysis of transmission electron microscopy images showed that the outer diameters of the N-CNTs decreased upon increasing the oxygen composition by mass in the synthesis precursors from 1 to 4 wt% oxygen, the oxygen was derived from ethylbenzoate. In addition, the scanning electron microscopy

and XRD revealed that the alignment of N-CNTs increased upon addition of oxygen. Electrical conductivity measurements of N-CNTs showed a negative relationship between the amount of oxygen in the starting materials and the conductivity of N-CNTs.

Introduction

Doping of carbon nanotubes (CNTs) with nitrogen to form nitrogen-doped carbon nanotubes (N-CNTs) offers an appropriate channel for improving the electronic and physical properties of CNTs [1, 2]. Furthermore, the aforementioned properties of N-CNTs can be improved by modulating their alignment and outer diameters (OD) [3]. Consequently, research is increasingly being focused on developing synthetic procedures that facilitate the control of the type of nitrogen species incorporated and nitrogen content, alignment and OD of N-CNTs during synthesis [4]. N-CNTs contain electron-rich nitrogen species such as pyridinic and pyridinic oxide [5] moieties, which enhance their electronic and physical properties. As a result, N-CNTs can be suitable for a wide range of applications as components in electronic [6] and field emission devices [7]. N-CNTs can also be used as catalysts or as metal catalyst supports [8]. For instance, well aligned N-CNTs have shown good field emission properties [9], while increasing the amount of pyridinic nitrogen in N-CNTs enhances the catalytic activity of Pd supported on N-CNTs [10].

One useful approach in increasing the percentage of nitrogen-doping and the nitrogen species incorporated into the tubes is the use of high nitrogen-containing organic precursors, such as mixtures of imidazole and acetonitrile together with organometallic catalysts during synthesis of

Electronic supplementary material The online version of this article (doi:10.1007/s10853-014-8675-4) contains supplementary material, which is available to authorized users.

L. M. Ombaka · P. G. Ndungu · V. O. Nyamori (✉)
School of Chemistry and Physics, University of KwaZulu-Natal,
Westville Campus, Private Bag X54001, Durban 4000,
South Africa
e-mail: nyamori@ukzn.ac.za

the N-CNTs [11]. In a similar manner, the level and type of nitrogen-doping can be increased by the use of nitrogen-containing organometallic compounds as catalysts together with nitrogen-containing carbon sources such as acetonitrile. For example, Nxumalo et al. [12] reported the use of nitrogen-containing ferrocenyl derivatives as catalysts, and as a source of carbon and nitrogen in the synthesis of N-CNTs. Another useful approach entails the incorporation of oxygen-containing compounds, such as alcohols and water, which act as oxidising agents during the synthesis of N-CNTs [4]. For instance, different ratios of alcohols and nitrogen-containing organic solvents have been used to control the nitrogen content and OD of N-CNTs [13].

Esters are volatile oxygen-containing organic compounds, which are usually less toxic especially when compared with alcohols such as methanol which is commonly used in CNTs synthesis. Their application as a source of oxygen and in the modulation of N-CNTs remains unexploited. In this account, ethylbenzoate was used as the choice ester because it contains a low ratio of O:C (2:9) making it a good source of low oxygen percentages. Additionally, ethylbenzoate is miscible with most organic solvent and also promotes the solubility of the ferrocenyl catalyst in toluene or acetonitrile. Hence, we report the use of different ratios of ethylbenzoate and acetonitrile to modulate the nitrogen content, OD, and alignment of N-CNTs. Also, we report for the first time the effect of increasing nitrogen-doping levels on the surface energy of N-CNTs. In addition, the chemical vapour deposition (CVD) method for the synthesis of N-CNTs using 3-ferrocenyl-2-(4-cyanophenyl)acrylonitrile as a catalyst, and also as a carbon and nitrogen source, is reported for the first time.

Experimental

Materials

Ferrocenecarboxaldehyde 98 %, 4-cyanophenylacetonitrile 97 %, piperidine 99 %, ethylbenzoate 99 %, diethyl ether 99.8 % and hexane 97 % were purchased from Sigma Aldrich. Acetonitrile 99.9 % and toluene 99.4 % were purchased from LiChroSolv. All reagents and solvents were of analytical grade and were used as received from the suppliers. Aluminium-backed silica gel 60 F₂₅₄ plates purchased from Merck were used to carry out thin layer chromatography in solvents of varying polarity. Purification of 3-ferrocenyl-2-(4-cyanophenyl)acrylonitrile by column chromatography was accomplished using Merck silica gel 60, 0.063–0.2 mm.

N-CNTs were synthesized in a quartz tube (inner diameter 27 mm, length 850 mm) placed in a muffle

furnace (Elite Thermal Systems Limited Model No. TSH12/50/610). The carrier gas used during synthesis of N-CNTs was 10 % hydrogen in argon (v/v) purchased from Airflex Industrial Gases. The rate of injection was controlled by a syringe pump (model no. NE-300, New Era Pump Systems Inc.).

Characterization

The catalyst, 3-ferrocenyl-2-(4-cyanophenyl)acrylonitrile, was characterized by the use of Fourier transform infrared spectroscopy (FTIR), nuclear magnetic resonance spectroscopy (NMR), mass spectroscopy and determination of its melting point. The melting point was determined using a Bibby Stuart Scientific model SMP3 apparatus. Infrared spectra were recorded on a PerkinElmer Universal ATR Spectrum 100 FTIR. The ¹H and ¹³C NMR spectra were recorded on a 400-MHz Bruker Ultrashield spectrometer at room temperature. A mass spectrum of the catalyst was obtained from a mass spectrometry (MS) with an electro-spray ionization (ESI).

Images of N-CNTs were taken using a transmission electron microscope (TEM) (JEOL JEM 1010) and a scanning electron microscope (SEM) (JEOL JSM 6100). A high-resolution TEM (JEOL 2100) was used to take higher magnification images of the N-CNTs. X-ray diffraction (XRD) spectra were obtained from a Rigaku D/max RB X-ray diffractometer equipped with graphite monochromatized high-intensity Cu K_α radiation ($\lambda = 0.15406$ nm). Elemental analysis was performed on a LECO CHNS-932 elemental analyzer, standardised with acetanilide. To determine the graphitic nature of the N-CNTs, a Raman spectrometer (DeltaNu Advantage 532TM) was used. The thermo-stability of N-CNTs was determined using a Q SeriesTM Thermal Analyzer DSC/TGA (Q600). The surface energy and acid–base properties were determined with an inverse gas chromatography surface energy analyzer (IGC-SEA) (SMS, Alperton, UK). Infrared spectra of N-CNTs embedded into KBr pellets were recorded on a PerkinElmer FTIR spectrometer spectrum RX1. The I–V properties of N-CNTs were determined using a four-point probe model connected to a digital micro voltmeter (DMV-001 Scientific Equipment ROORKEE), a low current source (LCS-02 Scientific Equipment ROORKEE) and a Proportional Integral Derivative (PID) controlled oven (PID 200).

Synthesis of 3-ferrocenyl-2-(4-cyanophenyl)acrylonitrile

The catalyst, 3-ferrocenyl-2-(4-cyanophenyl)acrylonitrile, was synthesized via a mechanochemical approach under solvent-free conditions following the procedure outlined by

Imrie et al. [14]. Ferrocenecarboxaldehyde (200.0 mg, 0.93 mmol) and 4-cyanophenylacetonitrile (132.0 mg, 0.93 mmol) were ground together in the presence of 2 drops of piperidine to yield a maroon paste. The paste was first dried in air, then under vacuum to obtain a maroon product. The maroon product was purified by means of column chromatography on silica gel with a solvent system of (1:1) hexane/diethyl ether to obtain 3-ferrocenyl-2-(4-cyanophenyl)acrylonitrile as dark red crystals. Yield (311.0 mg; yield of 98 %); m. p. 139 °C (lit [14] 140 °C). IR (cm^{-1}) 3099, 3050, 2943, 2225, 2207, 1609, 1585, 1452, 1408, 1367, 1312, 1252, 1178, 1103, 1032, 998, 920, 833, 826, 543, 501, 487, 432; ^1H NMR (ppm) in CDCl_3 : 7.68 (4H, s, ArH), 7.50 (1H, s, CH), 4.99 (2H, t, J 1.9, C_5H_4), 4.61 (2H, t, J 1.8, C_5H_4), 4.24 (5H, s, C_5H_5); ^{13}C NMR (ppm) in CDCl_3 132.85, 125.45, 146.60, 139.12, 118.56, 118.34, 111.36, 104.52, 77.18, 72.56, 70.68, 70.10. MS ($\text{C}_{20}\text{H}_{14}\text{FeN}_2$) ES: $[\text{M}]^+$ m/z calcd 338.050638, found 338.0500 (Supplementary Information S1).

Synthesis of N-CNTs

N-CNTs were synthesized by the use of a floating catalyst CVD method at 800, 850 and 900 °C. The CVD experimental setup and procedure used is described in detail elsewhere [15, 16]. Briefly, a flow rate of 0.8 mL min^{-1} was used to feed a solution of the precursors into a quartz tube which was placed in the middle of a tube furnace. The solution was carried through the quartz tube by a carrier gas made up of 10 % hydrogen in argon (v/v) which was pumped through the system at a rate of 100 mL min^{-1} at 80 kPa. The furnace was set to a reaction temperature of 800, 850 and 900 °C for 30 min, and the products were collected from the hot zone of the quartz tube upon completion of the reaction.

The compound, 3-ferrocenyl-2-(4-cyanophenyl)acrylonitrile, was used as a catalyst while acetonitrile or toluene was used as a carbon source. In addition to being a carbon source, acetonitrile also acted as a nitrogen source. The solution used to synthesize N-CNTs was made by dissolving 0.25 g of the catalyst in 9.75 g of acetonitrile or toluene to make a total of 10 g of solution (i.e. 2.5 wt% of catalyst).

In order to study the effect of oxygen during synthesis, acetonitrile was used as a carbon and nitrogen source at a synthesis temperature of 850 °C. To introduce varying amounts of oxygen into the synthesis precursors, 1, 2, 3 and 4 wt% of oxygen was derived from ethylbenzoate using the formula:

$$\text{wt\% oxygen} = \frac{\text{total weight of oxygen in } x \text{ g of ethylbenzoate}}{10 \text{ g}} \times 100,$$

where $x \text{ g} = 0.5, 1.0, 1.5$ or 2.0 g of ethylbenzoate.

Exactly 0.5, 1.0, 1.5 or 2.0 g of ethylbenzoate was added to 0.25 g of the catalyst and each solution was then prepared to a total mass of 10 g with acetonitrile. See Supplementary Information S2 for a summary of the oxygen and nitrogen percentages in acetonitrile solution. Prior to characterization, all N-CNTs were synthesized in triplicates and the products from the three runs were pooled together.

Electrical conductivity measurements

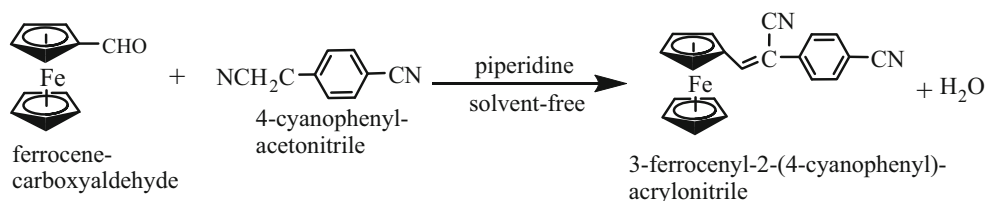
For I–V measurements, thin films of the N-CNTs were prepared based on modification of a previously reported vacuum filtration method [17]. In brief, 30 mg of N-CNTs was suspended in 10 mL of ethanol and sonicated for 30 min to form a homogeneous mixture. The mixture was vacuum filtered through Whatman filter paper. The filter paper containing the N-CNTs was then dried in an oven at 100 °C to evaporate excess ethanol and adsorbed water. The resulting film of supported N-CNTs was stored in a sealed container for further conductivity analysis. The thickness of the film was measured using a micrometre screw gauge. To determine the exact N-CNT film thickness, the thickness of the filter paper was subtracted from the thickness of the filter paper together with N-CNTs layer. As a control measure, I–V measurements were performed on the filter paper alone and this showed no conductivity.

Results and discussion

Synthesis of 3-ferrocenyl-2-(4-cyanophenyl)acrylonitrile

Mechanochemical grinding of ferrocenecarboxaldehyde and 4-cyanophenylacetonitrile in the presence of a catalytic amount of piperidine yielded 3-ferrocenyl-2-(4-cyanophenyl)acrylonitrile and water as a by-product (Scheme 1).

Upon grinding the reactants for 2 min, a melt was formed which turned into a solid after 5 min. Formation of the product was monitored by the use of thin layer chromatography, FTIR and NMR spectroscopy. Formation of the product was characterized by the disappearance of a sharp carbonyl absorption band ($\approx 1650 \text{ cm}^{-1}$) and the appearance of a strong nitrile absorption band ($\approx 2207 \text{ cm}^{-1}$) in the solid-state FTIR spectra. From the ^1H NMR spectra, formation of the product was marked by the disappearance of a carbonyl proton resonance peak ($\approx 10 \text{ ppm}$) and the appearance of an ethylene proton resonance peak ($\approx 7.5 \text{ ppm}$). This was further verified by the use of ^{13}C NMR spectra, in which the strong carbonyl carbon resonance peak ($\approx 190 \text{ ppm}$) disappeared, and MS confirmed that the compound was prepared.

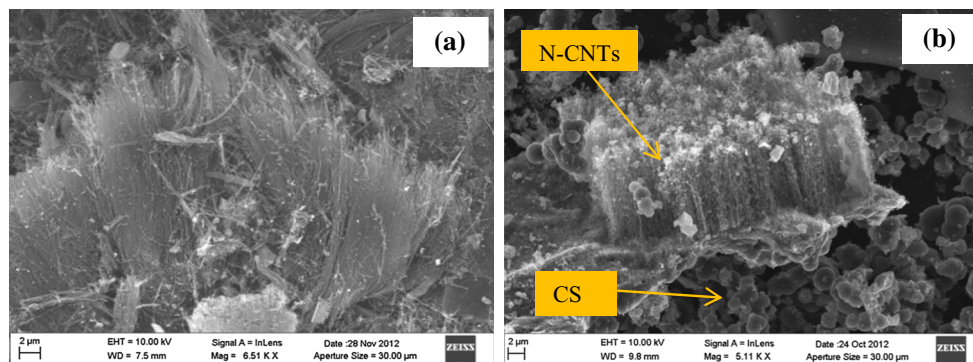
Scheme 1 Synthesis of 3-ferrocenyl-2-(4-cyanophenyl)acrylonitrile**Table 1** Product distribution of N-CNTs and carbon spheres obtained using either acetonitrile or toluene as the carbon source and 3-ferrocenyl-2-(4-cyanophenyl)acrylonitrile as the catalyst

Exp.	T_{\max} (°C)	Carbon source	N-CNTs %	Carbon spheres %	Amorphous carbon %
1					
a	900	Toluene	10	85	5
b	900	Acetonitrile	87	–	13
2					
a	850	Toluene	50	40	10
b	850	Acetonitrile	95	–	5
3					
a	800	Toluene	5	5	90
b	800	Acetonitrile	90	–	10

Exp experiment, T_{\max} maximum synthesis temperature

Effect of acetonitrile or toluene as carbon source on selectivity towards N-CNTs

The compound, 3-ferrocenyl-2-(4-cyanophenyl)acrylonitrile ($[M]^+$ m/z 338.0500), was used as a catalyst to synthesize N-CNTs in either acetonitrile or toluene. Synthesis conducted by the use of acetonitrile selectively yielded mainly N-CNTs (Table 1; Fig. 1a, 2a) and a small percentage of amorphous carbon while toluene yielded a mixture of N-CNTs and carbon spheres (CS) (Fig. 1b, 2b). From the TEM images of N-CNTs synthesized in acetonitrile or toluene, bamboo and cup-shaped compartments (see Fig. 2) associated with nitrogen-doping were evident [18].

Fig. 1 SEM images of N-CNTs synthesized at 850 °C using **a** acetonitrile and **b** toluene and 3-ferrocenyl-2-(4-cyanophenyl)acrylonitrile as the catalyst. Note that CS are only present in **(b)**

The selectivity towards formation of N-CNTs when acetonitrile is used can be explained by considering the decomposition products of toluene and acetonitrile as well as the carbon shell formation mechanism [19]. According to this mechanism, formation of N-CNTs or CS is controlled by two competing processes, i.e. the catalyst forward rate (V_s) and the carbon shell growth rate (V_p). When V_p is greater than V_s the formation of N-CNT is favoured, while when V_p is almost equal to or less than V_s a mixture of N-CNTs and CS is formed [20].

Acetonitrile decomposes to form hydrogen cyanide and methane in the gas phase as the first generation products [21]. These carbon species are light hydrocarbons that have been reported to be efficient sources of carbon material [22] resulting in V_p being higher than V_s which favours formation of N-CNTs. In addition, methane, which is a smaller molecule and also sp^3 hybridised is a better source of carbon than toluene. We would expect hydrogen cyanide (sp hybrid) with stronger bonds to be less favourable, but its small size makes it a lighter hydrocarbon compared to toluene (sp^2) which in turn makes it more suitable source of carbon [22]. On the contrary, toluene decomposes to form benzyl and phenyl radicals by losing atomic hydrogen and methyl, respectively [23]. The atomic hydrogen generated creates a hydrogen-rich surface on the catalyst that does not favour carbon growth. This results in V_p being equal to or less than V_s leading to formation of CS and N-CNTs. Additionally, the benzyl and phenyl radicals could act as nucleation sites to grow icosahedral shells which can roll up to form carbon spheres [22].

At 850 °C when either acetonitrile or toluene was used, the highest percentage of N-CNTs was obtained (Table 1,

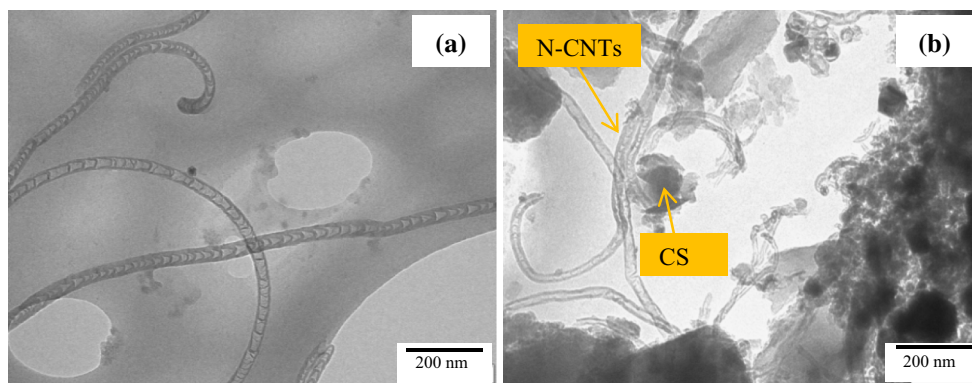


Fig. 2 TEM images of N-CNTs synthesized at 850 °C using **a** acetonitrile and **b** toluene and 3-ferrocenyl-2-(4-cyanophenyl)acrylonitrile as the catalyst

entries 2a and 2b). Also the use of toluene at a higher synthesis temperature (900 °C) yielded more carbon spheres than N-CNTs, while at a lower temperature (800 °C) mainly amorphous carbons were obtained (Table 1, entries 1a and 3a). Since acetonitrile was more selective than toluene at 850 °C, it was used to investigate the effect of oxygen during synthesis of N-CNTs at this temperature.

Effect of oxygen on the synthesized N-CNTs

Effect of oxygen on the yield of N-CNTs

Increasing of the oxygen wt% in the starting materials resulted in a decrease of the product yield (see Supplementary Information S3). Oxygen could be added up to 4 wt% while maintaining an effective growth of N-CNTs. Addition of 5 wt% oxygen resulted in formation of more amorphous carbons than N-CNTs while addition of 6 wt% oxygen resulted in no product formation. This was expected, considering that, at high temperatures, oxygen reacts with carbon present in the reaction chamber to form CO_x species, which exit the chamber as exhaust gases. Hence, as the weight oxygen percentage was increased, more carbon was converted to CO_x species reducing the carbon supply needed for N-CNT growth and resulting in a lower yield. As the weight oxygen percentage increased, the catalyst particle size also increased due to formation of larger Fe_3C particles (see “[Effect of oxygen on crystallinity and graphene interlayer spacing](#)” section). The larger Fe_3C particles may be poor catalysts for the initiation stage of N-CNT growth leading to lower N-CNT yields.

Effect of oxygen on nitrogen content of N-CNTs

The use of 3-ferrocenyl-2-(4-cyanophenyl)acrylonitrile in a solution of ethylbenzoate and acetonitrile at 850 °C yielded

N-CNTs with bamboo compartments as evidenced from the TEM images (Fig. 3).

From elemental analysis, the use of only acetonitrile yielded N-CNTs containing 6.4 wt% of nitrogen. The nitrogen-doping levels increased from 6.4 to 15.7 wt% upon addition of 1 wt% of oxygen to acetonitrile (Fig. 4). A further increase in the oxygen content (2–4 wt%) did not result in an additional increment of the nitrogen-doping level. Conventionally, the level of nitrogen-doping is expected to decrease with a decrease in the amount of nitrogen present in the precursors [24]. However, introduction of 1 wt% oxygen resulted in an increase in nitrogen-doping as the wt% of nitrogen in the precursors decreased. Oxygen is not doped into the tubes but can enhance the incorporation of pyridinic oxide species. The analysis shows that a low oxygen concentration (1 wt%) enhances nitrogen-doping of N-CNTs while higher concentrations of oxygen (2–4 wt%) do not favour it. In a similar manner, Bepete et al. [4], and Liu et al. [25] observed an increase in nitrogen-doping level in N-CNTs upon introduction of low oxygen concentrations using alcohols and water, respectively. A possible explanation is that, at low oxygen concentration (1 wt%), a favourable oxidative atmosphere is which reduces the concentration of reactive hydrogen species is formed. The reduction of hydrogen species promotes a conducive environment for faster chemisorption of nitrogen species into CNTs [26]. In contrast, higher oxygen concentrations (2–4 wt%) create a highly oxidative atmosphere that reacts with nitrogen species forming stable nitrogen dioxide and hence reducing the amount of nitrogen chemisorbed into N-CNTs.

Effect of oxygen on the morphology of N-CNTs

The OD of N-CNTs can be modulated by varying the levels of nitrogen-doping in N-CNTs. For example, Koós et al. reported a decrease in the OD of N-CNTs as a result of

Fig. 3 TEM images of N-CNTs synthesized at 850 °C by using **a** only acetonitrile, **b** 1 wt% oxygen in acetonitrile, **c** 2 wt% oxygen in acetonitrile, **d** 3 wt% oxygen in acetonitrile. The oxygen was derived from ethylbenzoate and the catalyst used was 3-ferrocenyl-2-(4-cyanophenyl)acrylonitrile

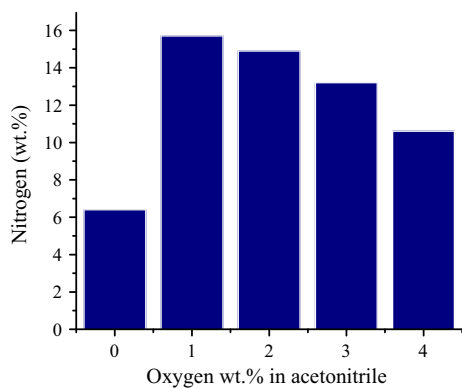
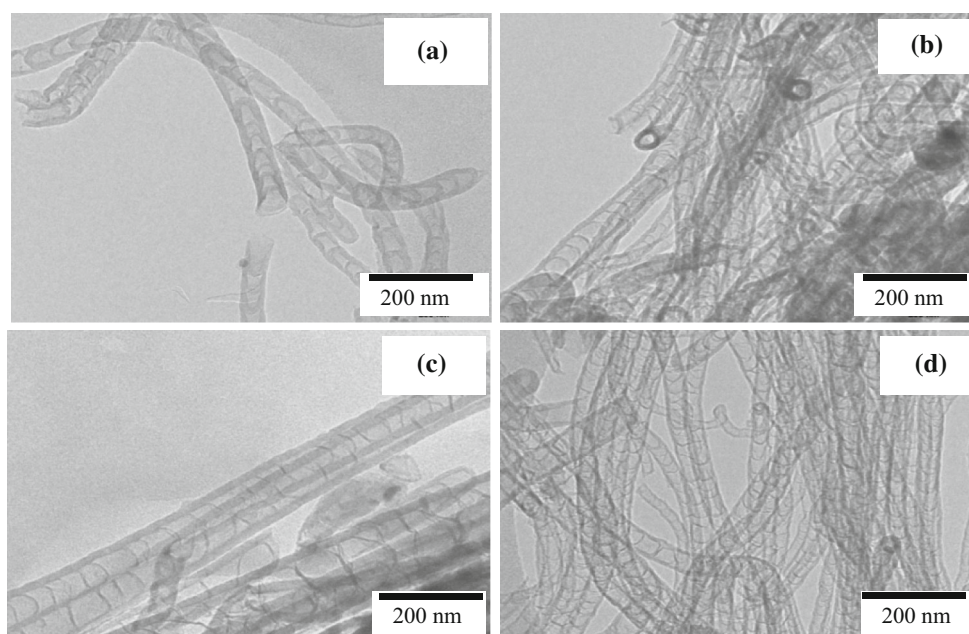


Fig. 4 Nitrogen content of N-CNTs synthesized using different wt% of oxygen derived from ethylbenzoate in acetonitrile at 850 °C

increased nitrogen-doping of CNTs [24]. This is because nitrogen species are predominant on the tube edges leading to closure of the tubes and making it unfavourable for further graphitic layering [27]. N-CNTs synthesized using 0–4 wt% oxygen in acetonitrile showed an average OD of 42–60 nm (Table 2).

The largest average OD was 60 nm from N-CNTs synthesized in acetonitrile only, while the smallest average OD was 42 nm from N-CNTs synthesized in the presence of 4 wt% of oxygen. In general, addition of 1–4 wt% of oxygen to acetonitrile resulted in a decrease of the OD. Since the nitrogen-doping levels directly correlate with OD, it is possible that the decrease in tube OD was due to an increase in nitrogen-doping (Fig. 4). This observation parallels those reported by Liu et al. who observed a constant decrease of tube OD with increase of nitrogen-doping in N-CNTs [11].

However, at higher oxygen concentrations (2–4 wt% oxygen), a further decrease in the OD of N-CNTs can be associated with etching of the outer walls. The etching effect on N-CNTs caused by high oxygen concentrations was observed from HR-TEM image analysis (Fig. 5).

Images of N-CNTs synthesized in higher oxygen contents (3–4 wt% oxygen) had evidence of partially formed tubes, serrated tube walls and reduced wall thickness (Fig. 5). This could imply that at higher oxygen concentration a highly oxidative atmosphere forms in the reaction chamber. The highly oxidative atmosphere etches the outer walls of the N-CNTs leading to formation of thinner tube walls. Another possible explanation is that oxygen forms a stable oxidised ring around the outer walls of N-CNTs. The stable oxidised ring hinders further deposition of carbon layers onto the outer walls of N-CNTs thus resulting in smaller OD [26]. In general, the wall thickness reduced as increasing amounts of oxygen were added to acetonitrile. The inner diameters of N-CNTs were observed to increase with increase in oxygen percentage. This increase in inner diameter can be attributed to an increase in the catalysts size (Fig. 6) as the oxygen percentage increased. As the catalyst size increases, its diameter also increases resulting in an increase in the size of the inner cavity of N-CNTs [28]. Ci et al. [29] who observed an increase in inner diameters of CNTs with increasing iron catalyst size made similar observations.

Effect of oxygen on crystallinity and graphene interlayer spacing

XRD characterization of CNTs gives useful information on structural strain, impurities, OD and distribution of

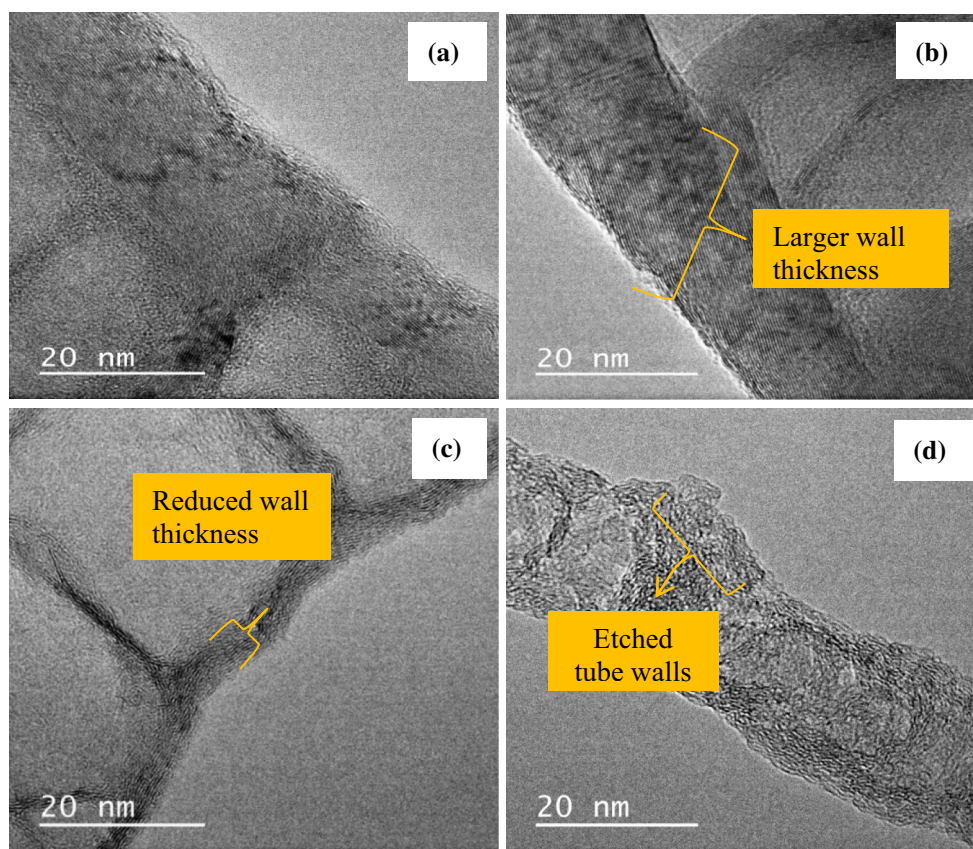
Table 2 Effect of oxygen on the morphology of N-CNTs synthesized using acetonitrile and ethylbenzoate at 850 °C and 3-ferrocenyl-2-(4-cyanophenyl)acrylonitrile as the catalyst

wt% oxygen	Ave. OD \pm SD (nm) ^a	Ave. ID \pm SD (nm) ^a	Ave. wall thickness \pm SD (nm) ^a	N-CNTs %	Amorphous carbon %
0	60 \pm 40	22 \pm 19	14 \pm 5	95	5
1	55 \pm 23	35 \pm 20	7 \pm 6	90	10
2	47 \pm 24	32 \pm 21	5 \pm 3	85	15
3	46 \pm 22	36 \pm 16	4 \pm 3	78	22
4	42 \pm 20	39 \pm 17	4 \pm 4	65	35

Ave. average, OD outer diameter, ID inner diameter, SD standard deviation

^a Experimentally measured values

Fig. 5 HR-TEM images of N-CNTs synthesized at 850 °C using **a** only acetonitrile, **b** 1 wt% oxygen, **c** 3 wt% oxygen and **d** 4 wt% oxygen in acetonitrile and 3-ferrocenyl-2-(4-cyanophenyl)acrylonitrile as the catalyst



chirality in CNTs [30]. The intensity and width of the C_{002} reflection of graphene can be associated with various microstructural parameters of N-CNTs, namely: the number of graphene layers, variations of the interlayer spacing, lattice distortions, tube OD, tube alignment and crystallinity of the graphene layers [31]. The XRD patterns of N-CNTs are similar to that of graphite and comprise of a graphite-like peak (C_{002}) associated with the interlayer spacing of graphene and a family of ($C_{h,k,l}$) peaks caused by the honeycomb lattice of a single graphene sheet [30].

The diffractograms of N-CNTs synthesized using 0–4 wt% oxygen in acetonitrile are shown in Fig. 6. For all diffractograms, the peak at $2\theta = 26.4^\circ$ showed a strong

intensity and it was indexed as the $C_{(002)}$ reflection of graphite [31]. The $C_{(002)}$ peak of N-CNTs synthesized using acetonitrile alone was sharper and narrower compared with the $C_{(002)}$ peaks of N-CNTs synthesized in the presence of oxygen. Additionally, the full widths at half maxima (FWHM) of the $C_{(002)}$ peaks increased linearly with increase in oxygen content in the precursors (Table 3).

Broadening of the FWHM of the $C_{(002)}$ peak can either be due to a decrease in crystallinity caused by an increase in the nitrogen-doping levels, or a decrease in OD of the N-CNTs. An increase in nitrogen-doping increases the structural strain by increasing the surface defects on the regular graphite layers of the CNTs leading to broadening

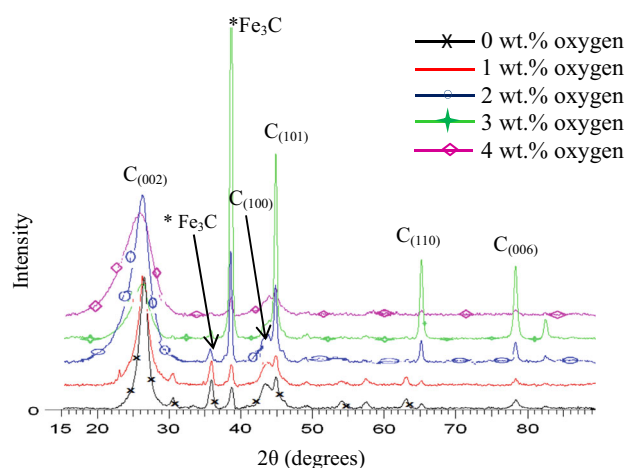


Fig. 6 XRD diffractograms of N-CNTs synthesized using 0–4 wt% oxygen in acetonitrile at 850 °C using 3-ferrocenyl-2-(4-cyanophenyl)acrylonitrile as the catalyst. The residual iron carbide from the catalyst is symbolised by an *asterisk*

Table 3 X-ray structural parameters of N-CNTs synthesized using 0–4 % oxygen in acetonitrile at 850 °C and 3-ferrocenyl-2-(4-cyanophenyl)acrylonitrile as the catalyst

wt% oxygen	FWHM of $C_{(002)}$ peak (°)	Intensity of $C_{(002)}$ peak	Interlayer spacing of $C_{(002)}$ peak (nm)	Intensity of Fe_3C peak	Interlayer spacing of Fe_3C (nm)
0	1.258	8113	0.3369	3810	0.2328
1	1.519	6425	0.3386	3833	0.2330
2	1.847	4921	0.3407	6577	0.2335
3	2.794	3135	0.3464	23260	0.2332
4	4.296	6053	0.3506	923	0.2331

FWHM full width at half maximum

of the FWHM [32]. Hence, N-CNTs synthesized in the presence of acetonitrile alone, which had a smaller FWHM were considered more crystalline than those synthesized in the presence of oxygen [33].

Likewise, broadening of the $C_{(002)}$ peak can be induced by an increase in structural strain resulting from changes in the interlayer spacing (d-spacing). The d-spacing of the synthesized N-CNTs was ≈ 0.34 nm (Table 3) which is comparable to those documented in previous reports [34, 35]. From XRD analysis, the value of the calculated d-spacing was observed to increase with a decrease in the tube OD and wall thickness caused by the addition of oxygen. Previous studies have shown that as the tube OD decreases, the number of walls reduces and the curvature of the tube walls increases resulting in increased strain in the nanotubes [35]. The increase in strain brings about columbic repulsions between like charges on the walls resulting in an increased d-spacing and FWHM. On the

contrary, as the tube OD increase, the wall curvature decreases leading to a decrease of strain in the nanotubes. This results in an increased interaction between the walls leading to a decrease of the d-spacing. Hence, the increase in d-spacing and FWHM resulting from a decrease in tube OD and wall thickness was consistent with observations in the literature [35]. The intensity of the $C_{(002)}$ peak showed a correlation with the alignment of N-CNTs which is discussed in “Effect of oxygen on alignment of N-CNTs” section

A peak at $\approx 38.6^\circ$ with an interlayer spacing of ≈ 0.23 nm was observed in all the diffractograms and it was indexed as the Fe_3C reflection [36]. The presence of Fe_3C peak could imply that Fe_3C was the predominant catalytic phase during N-CNTs growth as suggested by Wirth et al. [37]. From the diffractograms, addition of 1–3 wt% of oxygen did not hamper the formation of Fe_3C , but instead promoted it as the peak intensity increased when 1–3 wt% of oxygen was used. This increment in residual iron carbide was also evidenced from the thermogravimetric curves of N-CNTs (Fig. 8) which showed an increase in the residual weight when 1–3 wt% of oxygen was used. However, addition of 4 wt% oxygen resulted in a sharp decrease in the intensity of the Fe_3C peak and the residual weight of N-CNTs. This could imply that addition of 4 wt% oxygen retarded the formation of Fe_3C . Furthermore, as the Fe_3C reflection intensity increased, the $C_{(002)}$ intensity was observed to decrease monotonically. This could imply that the crystallinity of Fe_3C influenced the intensity of $C_{(002)}$ peak.

Effect of oxygen on the graphitic nature of N-CNTs

The graphitic nature of the N-CNTs was determined using Raman spectroscopy. The Raman spectra of all synthesized N-CNTs showed two first order peaks, i.e. a disorder band (D-band) at 1345 – 1367 cm^{-1} and a graphitic band (G-band) at 1553 – 1601 cm^{-1} (Fig. 7a). The D-band corresponds to the A_{1g} breathing modes of disordered carbon networks, while the G-band corresponds to splitting of the E_{2g} stretching modes of graphitic carbon networks [38]. The ratio of the integrated area of the D-band to that of the G-band (I_D/I_G) was used to determine the level of disorder in N-CNTs [39, 40].

Doping of CNTs with nitrogen introduces disorder in the regular graphite layers of CNTs, hence an increase in the nitrogen-doping of CNTs results in an enhanced D-band leading to a higher I_D/I_G ratio [41]. The I_D/I_G ratios of the N-CNTs increased when 1 wt% oxygen was used, however, upon addition of 2–4 wt% oxygen, the I_D/I_G ratio decreased but retained a value higher than that of N-CNTs synthesized without oxygen (Fig. 7b). The higher I_D/I_G ratio of N-CNTs synthesized in the presence of oxygen

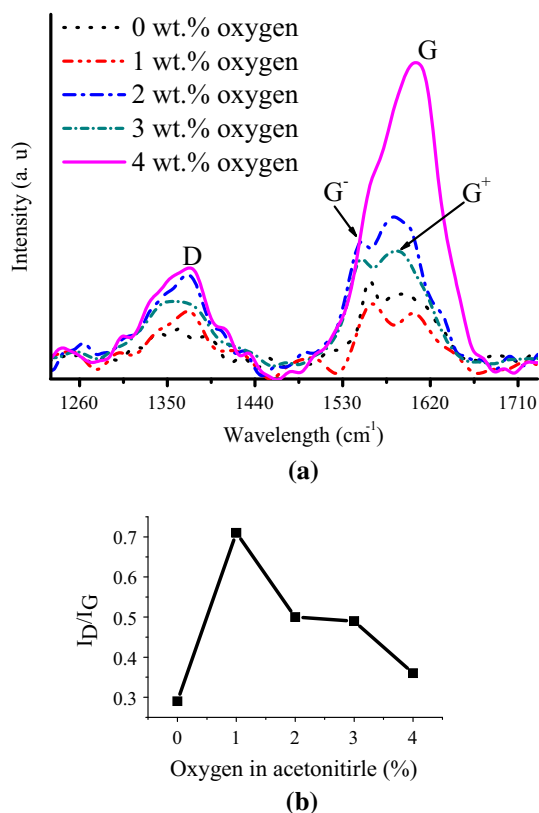


Fig. 7 **a** Raman spectra and **b** I_D/I_G ratios of N-CNTs synthesized using 0–4 wt% of oxygen in acetonitrile at 850 °C and 3-ferrocenyl-2-(4-cyanophenyl)acrylonitrile as the catalyst

indicates that addition of oxygen increased nitrogen-doping which in turn increased the structural defects in N-CNTs [42]. This increase in structural defects can be attributed to an increased disturbance of perfect hexagonal structure and layering of the graphene sheets due to introduction of pentagons or heptagons [41]. The observations made from Raman spectroscopy were in good agreement with the nitrogen content derived from elemental analysis of the synthesized N-CNTs (cf. Figure 7b, 4).

From the Raman spectra, the G-bands of all N-CNTs were split into two peaks at ≈ 1553 and ≈ 1601 cm^{-1} associated with the G^- and G^+ modes, respectively. The G^- mode arises from atomic displacement along the circumferential direction and it is indicative of the presence of metallic CNTs [43]. The G^+ mode arises from atomic displacement along the tube axis and it is related to the chirality of N-CNTs [44]. As the amount of oxygen in acetonitrile increased from 0 to 4 wt%, the G^- peak diminished while the G^+ peak intensified. Diminishing of the G^- peak indicated that increasing the amount of oxygen decreased the abundance of metallic N-CNTs [43]. While the increase in intensity of the G^+ peak implied that as the percentage of oxygen increased the chirality of N-CNTs changed from a low chiral angle (zigzag) to a high

chiral angle (armchair) [44]. This shift is attributed to an increase in the comprehensive strain of the C–C bonds or C–C–C angles in the graphene structures as the OD of the N-CNTs decrease and the curvature increases; which is in agreement with our XRD analysis [45].

The G-band of N-CNTs synthesized with 4 wt% oxygen was mainly composed of the G^+ peak and a very weak G^- peak appearing as a peak shoulder. This resulted in a more symmetrical G-band, showing an exceptionally high intensity relative to the D-band (Fig. 7a). The high G-band intensity could be indicative of a single peak component arising from N-CNTs with a homogenous low OD and a single chirality. CNTs with small OD (≤ 10 nm) have been reported to exhibit a strong G-band intensity compared with the D-band intensity [35]. Also, the Raman spectra of N-CNTs synthesized with 4 wt% oxygen showed peaks at 296.5 and 310.6 cm^{-1} (see Supplementary Information S4). These peaks can be attributed to the radial breathing mode (RBM) of the thin walled tubes present in this sample. These observations are analogous to those made from the Raman spectra of single-walled CNTs (SWCNTs), which exhibit a RBM and a very strong G-band compared to the D-band [30].

Effect of oxygen on the thermal stability of N-CNTs

Thermal stability of N-CNTs was investigated by the use of TGA analysis. The thermograms and derivative thermograms (DTG) are shown in Fig. 8. From the thermograms and DTG, it can be deduced that N-CNTs synthesized with oxygen in acetonitrile exhibit a lower initial decomposition temperature (≈ 420 °C) compared with N-CNTs synthesized in acetonitrile only (≈ 510 °C). The thermal stability of N-CNTs was also observed to decrease as the amount of oxygen in acetonitrile increased (Fig. 8a). This decrease in thermal stability can be attributed to an increase in defects introduced by the nitrogen-doping level. Such defects can act as hot spots in the sample, which initiate decomposition at lower temperatures, and thus result in a lower thermal stability of N-CNTs [46].

Addition of oxygen also lead to an increase in the amount of amorphous carbons (Table 2) which are less thermally stable and hence possess a lower initial decomposition temperature. The DTG of N-CNTs synthesized with 1–4 wt% oxygen in acetonitrile revealed the appearance of peaks (marked by a dashed line) at ≈ 420 °C upon introduction of oxygen. These peaks are ascribed to the presence of amorphous carbons. The derivative weight of these peaks was observed to increase as the amount of oxygen incorporated into acetonitrile increased. In contrast, the derivative weight of the peaks at ≈ 510 °C (marked with a continuous line), which are associated with N-CNTs, was observed to decrease with a decrease in oxygen

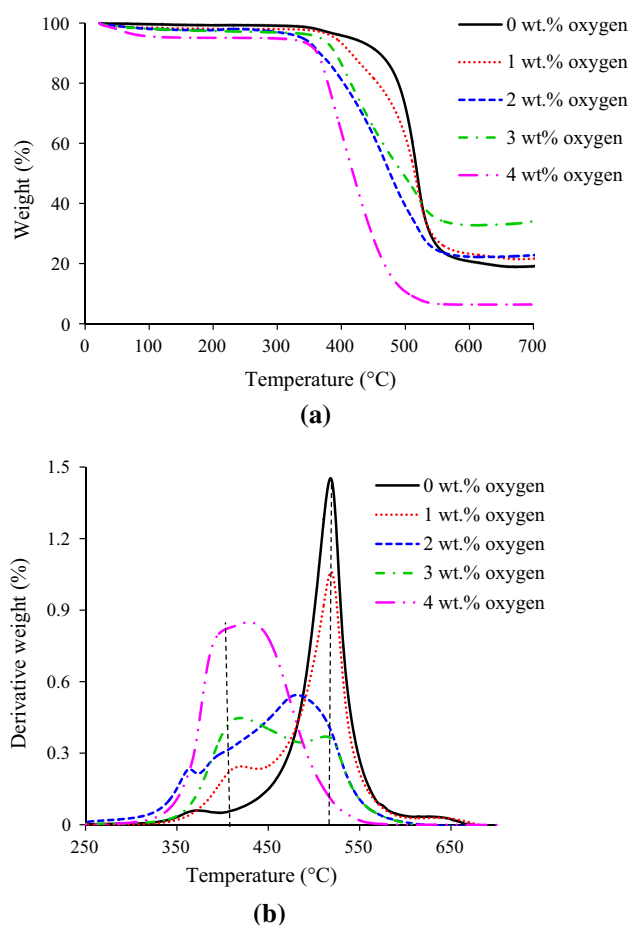


Fig. 8 **a** Thermograms and **b** derivative thermograms of N-CNTs synthesized using 0–4 wt% of oxygen in acetonitrile at 850 °C and 3-ferrocenyl-2-(4-cyanophenyl)acrylonitrile as the catalyst

content. This could imply that as the oxygen percentage is increased the amount of amorphous carbons increases leading to an overall decrease in thermal stability of N-CNTs [47]. Similar observations were made from TEM analysis summarised in Table 2 whereby the distribution of amorphous carbon increased with the increase of oxygen content. The trend of decreasing thermostability from TGA analysis concurred with the increase in FWHM observed from XRD analysis.

Effect of oxygen on alignment of N-CNTs

The alignment of N-CNTs was determined from the SEM images and analysis of wide-angle XRD diffraction patterns. For each sample, at least twenty SEM images of N-CNTs were analysed and the representative images are shown in Fig. 9. From the SEM images, N-CNTs synthesized using acetonitrile mainly showed a tangled morphology, while N-CNTs synthesized using 1–4 wt% of oxygen in acetonitrile mainly showed an aligned morphology. For example, vertically aligned N-CNTs with

open tube-ends were observed from the SEM images of N-CNTs grown from 3 wt% of oxygen (Fig. 9c).

The degree of alignment of N-CNTs was also determined by evaluating the intensity of the $C_{(002)}$ peak of the N-CNTs from the XRD diffraction patterns. Cao et al. reported that the intensity of the $C_{(002)}$ peak decreases as the alignment of CNTs increases [48]. From our results, the $C_{(002)}$ peak intensities of N-CNTs synthesized using 0–3 wt% of oxygen were seen to decrease with an increase in oxygen content (Fig. 6; Table 3). This could imply that the degree of N-CNT alignment increased with an increase of oxygen content from 0 to 3 wt%. Thus, the trend of the variation in the alignment of the N-CNTs observed from the XRD analysis supported the trend observed from the SEM images. Since oxygen possesses a ‘cleaning effect’ on as-grown CNTs [49], it is possible that incorporation of a low oxygen content brings about etching of the outer walls of CNTs resulting in the formation of more aligned N-CNTs.

Effect of oxygen on the surface chemistry of N-CNTs

The surface chemistry of N-CNTs was investigated by means of inverse gas chromatography (IGC)-surface energy analysis and FTIR. From the IGC analysis, addition of oxygen to acetonitrile modified the surface energy and acid–base properties of the N-CNTs (Table 4). The dispersive surface energy (γ_s^D) of N-CNTs was determined using the Doris and Gray method [50]. N-CNTs synthesized in the presence of oxygen showed an appreciably high γ_s^D ($>70 \text{ mJm}^{-2}$) which was higher than the γ_s^D of N-CNTs synthesized with acetonitrile only (Table 4). The increased γ_s^D of N-CNTs synthesized using oxygen was attributed to an increase in: surface defects on the graphene layers, nitrogen-containing functional groups with high γ_s^D and open tube ends [51]. Similar observations were also made from elemental analysis and Raman spectroscopy.

The surface acid–base properties of N-CNTs were evaluated using dichloromethane, acetonitrile and ethyl acetate as the polar probes. To compare the surface basicity of different N-CNTs, the Lewis base constant K_b was used [52]. The basic constant (K_b) of N-CNTs synthesized in the presence of oxygen was higher than that of N-CNTs synthesized with acetonitrile only (Table 4). This suggests that the surface of N-CNTs synthesized in the presence of oxygen contained more basic functionalities than that of N-CNTs synthesized in acetonitrile only [5].

The FTIR spectra of N-CNTs synthesized using 0–4 wt% oxygen in acetonitrile is presented in Fig. 10. A broad band at 3427 cm^{-1} was observed in all spectra and it was consistent with the –OH stretching vibration of hydrogen bonded alcohols or carboxylic acids [45]. Since the band at 1723 cm^{-1} attributed to the C=O group was

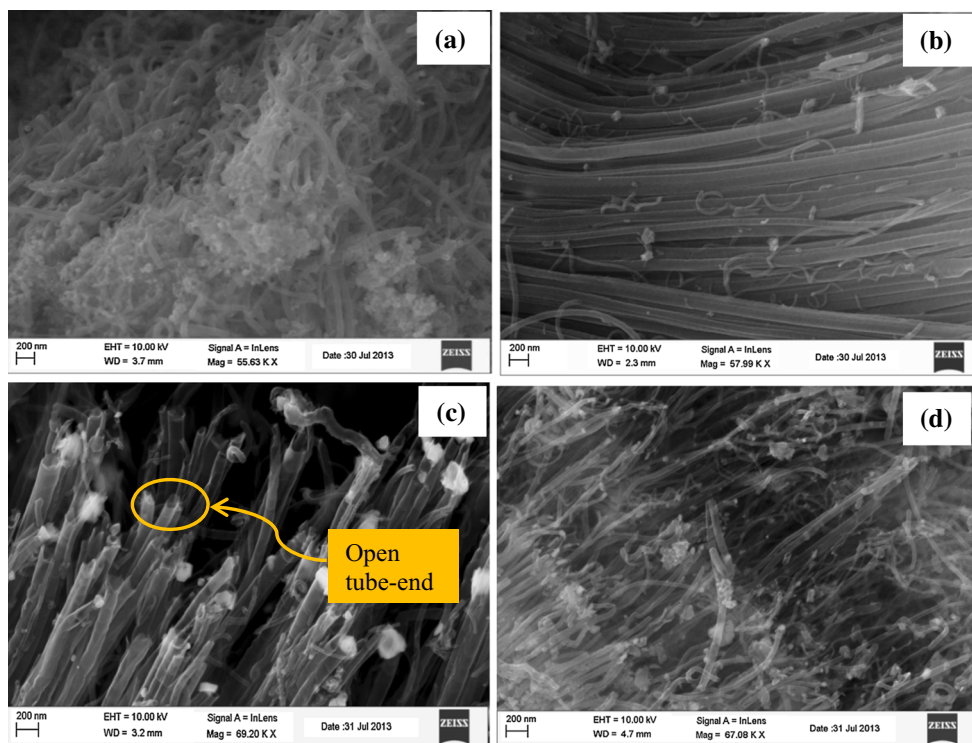


Fig. 9 SEM images of N-CNTs synthesized using **a** only acetonitrile, **b** 1 wt% oxygen, **c** 3 wt% oxygen and **d** 4 wt% oxygen in acetonitrile at 850 °C and 3-ferrocenyl-2-(4-cyanophenyl)acrylonitrile as the catalyst. Note the difference in alignment of N-CNTs in (a, b)

Table 4 Surface energy and surface chemistry of selected N-CNTs synthesized at 850 °C using 3-ferrocenyl-2-(4-cyanophenyl)acrylonitrile as the catalyst

wt% oxygen	Nitrogen (wt%)	Surface energy (γ_s^D) mJm ⁻²	K _a	K _b	K _a /K _b
0	6.4	34	0.0500	0.3888	0.1286
1	15.7	112	0.1121	0.7183	0.1560
2	14.9	78	0.0818	0.6432	0.1272

weak, the broad peak at 3427 cm⁻¹ was ascribed to alcohols. The peaks at 2949 and 2871 cm⁻¹ were designated as the stretching vibration of CH₂ and CH₃ groups [53]. The peak at 2381 cm⁻¹ was designated as the stretching vibrations of C–O groups [54]. The aromatic stretching modes of the C=C present in the graphene structure of CNTs were observed at 1678 cm⁻¹, while the C–H vibration modes were assigned to the peaks at 788 and 699 cm⁻¹ [53]. The presence of N-CNTs was evidenced by the existence of peaks at 1567, 1389 and 1110 cm⁻¹ assigned to stretching vibrations of C=N, C–NH₃ and C–N functional groups, respectively [2, 54–56].

Doping of CNTs with nitrogen results in substitution of an sp² carbon with nitrogen to form C=N or C–N bonds showing IR activity [54]. The intensity of the peak at 1567 cm⁻¹ assigned to the C=N group was observed to

increase when 1–4 wt% oxygen in acetonitrile was used to synthesize N-CNTs. For N-CNTs synthesized without oxygen, the intensity of the C=N band at 1567 cm⁻¹ was smaller than that of the C=C band at 1678 cm⁻¹. On the contrary, for N-CNTs synthesized using 1–4 wt% oxygen the intensity of the C=N band at 1567 cm⁻¹ was larger than that of the C=C band at 1678 cm⁻¹. This increase in intensity of the C=N peak at 1567 cm⁻¹ can be related to an increase in nitrogen-doping level, which was also observed from elemental analysis. The increase in density of C=N functional groups observed from the FTIR spectra could be related to an increase of basic functional groups such as pyridinic or pyridinic oxide species as observed from the IGC analysis. Such N-CNTs can be used as metal-free catalysts or as metal catalyst supports [8].

Effect of oxygen on the conductivity of N-CNTs

The conductivity of all N-CNTs was determined by the use of a four-point probe within a temperature range of 296–383 K. To calculate the conductivity (σ) in S m⁻¹, the following equation was used:

$$\text{conductivity } (\sigma) = \frac{1}{[\rho]} \quad \text{and} \quad \rho = \frac{\pi h}{\ln 2} \left[\frac{\Delta V}{I} \right],$$

where ρ is the resistivity, h is the film thickness, ΔV is the change in voltage and I is the measured current.

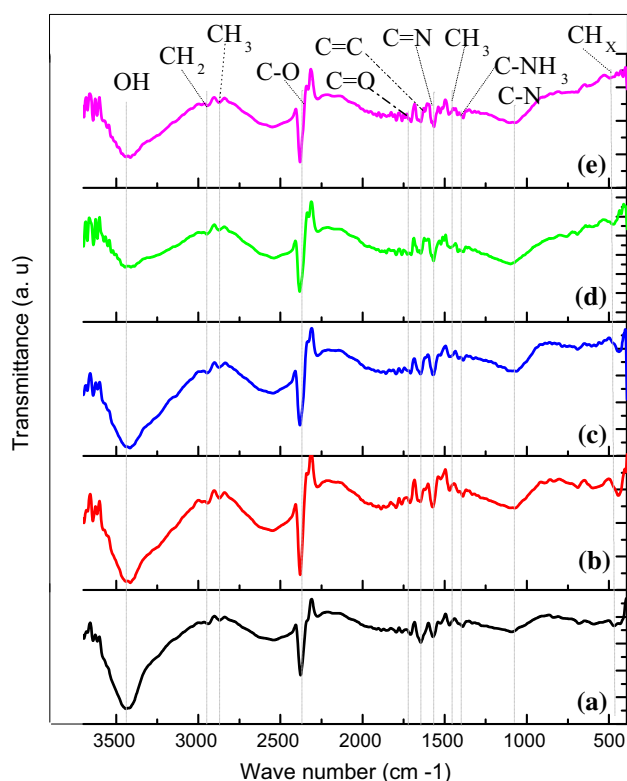


Fig. 10 FTIR spectra of N-CNTs synthesized using (a) only acetonitrile, (b) 1 wt% oxygen, (c) 2 wt% oxygen, (d) 3 wt% oxygen and (e) 4 wt% oxygen in acetonitrile at 850 °C and 3-ferrocenyl-2-(4-cyanophenyl)acrylonitrile as the catalyst

For all N-CNTs, a buckypaper (compact film) was obtained by pressurising the N-CNTs to a similar film thickness. The electrical properties of buckypapers are dependent on the inter-tube interactions between individual N-CNTs, nanotube junctions, length of the N-CNTs, purity, type, and preparation techniques [57]. High inter-tube interactions improve the overall electrical properties of N-CNTs by minimizing the internal resistance [58]. To improve the inter-tube interactions of the intermingled N-CNTs, a high pressure which was also consistent was used during formation of the buckypaper.

The conductivity of all N-CNTs increased with increase in temperature implying that the samples exhibited semi-conducting properties (Fig. 11).

Increasing the amount of oxygen in acetonitrile from 0 to 4 wt% resulted in a decrease of conductivity. This decrease in conductivity was directly related with the decrease of N-CNTs OD and N-CNTs junctions resulting from addition of 0–4 wt% oxygen. As the OD and junctions of N-CNTs decreased, the mean free path of charge carriers also decreased therefore decreasing the conductivity of N-CNTs [59]. Additionally, as the OD decreases the columbic repulsion between graphene layers of N-CNTs increases (see “[Effect of oxygen on crystallinity and graphene interlayer spacing](#)” section). The increased

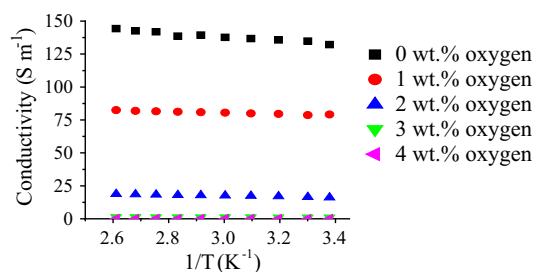


Fig. 11 Conductivity of N-CNTs synthesized at 850 °C using 0–4 wt% oxygen in acetonitrile and 3-ferrocenyl-2-(4-cyanophenyl)acrylonitrile as the catalyst

columbic repulsion can induce polarisation effects, which may block transmission of electrons by increasing the resistance in N-CNTs and in turn reducing the current flow in N-CNTs. Ibrahim et al. [5], who reported a decrease in conductivity as the tube OD decreased and the nitrogen doping levels increased, made similar observations.

Conclusions

We have reported the successful synthesis of N-CNTs using 3-ferrocenyl-2-(4-cyanophenyl)acrylonitrile as a novel catalyst. The use of acetonitrile as a carbon source selectively formed only N-CNTs while the use of toluene as a carbon source yielded a mixture of N-CNTs and carbon spheres. Selectivity towards N-CNTs formation was accredited to the decomposition products of acetonitrile when used as a carbon source. The results obtained demonstrate that nitrogen-containing organometallic compounds are versatile catalysts for synthesis of N-CNTs because they act as catalysts and as a nitrogen source. We have also demonstrated a simple approach of tuning the nitrogen content, surface energy, surface basicity, alignment, and conductivity of N-CNTs by adding a low concentration of oxygen derived from an ester, namely, ethylbenzoate. The bulk electronic and physical properties of N-CNTs were strongly influenced by the OD of N-CNTs that was modulated by adding oxygen to acetonitrile. Low oxygen concentrations were favourable for the growth of well-aligned N-CNTs containing higher levels of nitrogen. However, there is a need to conduct further studies to determine the mechanism by which low oxygen concentrations influence the physicochemical properties of N-CNTs.

Supplementary material

Supplementary Material Available: Tables detailing mole ratios used during synthesis and data obtained from yields of products. A figure obtained from Raman spectroscopy.

Acknowledgements The National Research Foundation (NRF) and University of KwaZulu-Natal (UKZN) financed this research. We are grateful to Prof B. S. Martincigh, Dr. N. Nombona and Dr. R. S. Mwakubambanya, for assisting in proof-reading the manuscript and their critical comments of the manuscript.

References

- Ionescu MI, Zhang Y, Li R, Abou-Rachid H, Sun X (2012) Nitrogen-doping effects on the growth, structure and electrical performance of carbon nanotubes obtained by spray pyrolysis method. *Appl Surf Sci* 258:4563
- Ritter U, Tsierkezos NG, Prylutskyy YI, Matzui LY, Gubanov VO, Bilyi MM, Davydenko MO (2012) Structure–electrical resistivity relationship of N-doped multi-walled carbon nanotubes. *J Mater Sci* 47:2390. doi:10.1007/s10853-011-6059-6
- Liu H, Zhang Y, Li R, Sun X, Abou-Rachid H (2011) Effects of bimetallic catalysts on synthesis of nitrogen-doped carbon nanotubes as nanoscale energetic materials. *Particuology* 9:465
- Bepete G, Tetana ZN, Lindner S, Rümmele MH, Chiguvare Z, Coville NJ (2013) The use of aliphatic alcohol chain length to control the nitrogen type and content in nitrogen doped carbon nanotubes. *Carbon* 52:316
- Ibrahim EMM, Vyacheslav OK, Leonhardt A, Hampel S, Oswald S, Rümmele MH, Büchner B (2010) Synthesis, characterization, and electrical properties of nitrogen-doped single-walled carbon nanotubes with different nitrogen content. *Diamond Relat Mater* 19:1199
- Jana D, Sun C-L, Chen L-C, Chen K-H (2013) Effect of chemical doping of boron and nitrogen on the electronic, optical, and electrochemical properties of carbon nanotubes. *Prog Mater Sci* 58:565
- Lai Y-H, Lian H-B, Lee K-Y (2009) Field emission of vertically aligned carbon nanotubes with various content of nitrogen. *Diamond Relat Mater* 18:544
- Ombaka LM, Ndungu P, Nyamori VO (2013) Usage of carbon nanotubes as platinum and nickel catalyst support in dehydrogenation reactions. *Catal Today* 217:65
- Padya B, Kalita D, Jain PK, Padmanabham G, Ravi M, Bhat KS (2013) Nitrogen incorporated highly aligned carbon nanotube arrays thin film grown from single feedstock for field emission. *J Nanoelectron Optoe* 8:177
- Chizari K, Janowska I, Houllé M, Florea I, Ersen O, Romero T, Bernhardt P, Ledoux MJ, Pham-Huu C (2010) Tuning of nitrogen-doped carbon nanotubes as catalyst support for liquid-phase reaction. *Appl Catal A* 380:72
- Liu J, Zhang Y, Ionescu MI, Li R, Sun X (2011) Nitrogen-doped carbon nanotubes with tunable structure and high yield produced by ultrasonic spray pyrolysis. *Appl Surf Sci* 257:7837
- Nxumalo EN, Chabalala VP, Nyamori VO, Witcomb MJ, Coville NJ (2010) Influence of methylimidazole isomers on ferrocene-catalysed nitrogen doped carbon nanotube synthesis. *J Organomet Chem* 695:1451
- Thurakitsee T, Kramberger C, Zhao P, Aikawa S, Harish S, Chiashi S, Einarsson E, Maruyama S (2012) Diameter-controlled and nitrogen-doped vertically aligned single-walled carbon nanotubes. *Carbon* 50:2635
- Imrie C, Kleyi P, Nyamori VO, Gerber TIA, Levendis DC, Look J (2007) Further solvent-free reactions of ferrocenylaldehydes: synthesis of 1,10-ferrocenyldiimines and ferrocenylacrylonitriles. *J Organomet Chem* 692:3443
- Oosthuizen RS, Nyamori VO (2012) Heteroatom-containing ferrocene derivatives as catalysts for MWCNTs and other shaped carbon nanomaterials. *Appl Organomet Chem* 26:536
- Nyamori VO, Nxumalo EN, Coville NJ (2009) The effect of arylferrocene ring substituents on the synthesis of multi-walled carbon nanotubes. *J Organomet Chem* 694:2222
- Trancik JE, Barton SC, Hone J (2008) Transparent and catalytic carbon nanotube films. *J Nano Lett* 8:982
- Chen L, Xia K, Huang L, Li L, Pei L, Fei S (2013) Facile synthesis and hydrogen storage application of nitrogen-doped carbon nanotubes with bamboolike structure. *Int J Hydrogen Energy* 38:3297
- Kovalevski VV, Safronov AN (1998) Pyrolysis of hollow carbons on melted catalyst. *Carbon* 36:963
- Zhang C, Lv M, Wang X, Li J, Yang X, Yang J, Hu H (2013) Controllable synthesis and formation mechanism of carbon micro/nano-structural materials. *Chem Phys Lett* 586:121
- Lifshitz A, Tamburu C (1999) Thermal decomposition of acetonitrile. Kinetic modeling. *Int J Chem Kinet* 30:341
- Shaikjee A, Coville NJ (2012) The role of the hydrocarbon source on the growth of carbon materials. *Carbon* 50:3376
- Derudi M, Polino D, Cavallotti C (2011) Toluene and benzyl decomposition mechanisms: elementary reactions and kinetic simulations. *Phys Chem Chem Phys* 13:21308
- Koós AA, Dowling M, Jurkschat K, Crossley A, Grobert N (2009) Effect of the experimental parameters on the structure of nitrogen-doped carbon nanotubes produced by aerosol chemical vapor deposition. *Carbon* 47:30
- Liu S, Zhang Y, Lin Y, Zhao Z, Li Q (2014) Tailoring the structure and nitrogen content of nitrogen-doped carbon nanotubes by water-assisted growth. *Carbon* 69:247
- Rümmele MH, Borowiak-Palen E, Gemming T, Pichler T, Knupfer M, Kalbác M, Dunsch L, Jost O, Silva SRP, Pompe W, Büchner B (2005) Novel catalysts, room temperature, and the importance of oxygen for the synthesis of single-walled carbon nanotubes. *Nano Lett* 5:1209
- Sumpter BG, Meunier V, Romo-Herrera JM, Cruz-Silva E, Cullen DA, Terrones H, Smith DJ, Terrones M (2007) Nitrogen-mediated carbon nanotube growth: diameter reduction, metallicity, bundle dispersability, and bamboo-like structure formation. *ACS Nano* 1:369
- Jourdain V, Bichara C (2013) Current understanding of the growth of carbon nanotubes in catalytic chemical vapour deposition. *Carbon* 58:2
- Ci L, Vajtai R, Ajayan PM (2007) Vertically aligned large-diameter double-walled carbon nanotube arrays having ultralow density. *J Phys Chem C* 111:9077
- Belin T, Epron F (2005) Characterization Methods of carbon nanotubes: a review. *Mater Sci Eng B* 119:105
- Lambin P, Loiseau A, Culot C, Biro L (2002) Structure of carbon nanotubes probed by local and global probes. *Carbon* 40:1635
- Chiang YC, Lin W-H, Chang Y-C (2011) The influence of treatment duration on multi-walled carbon nanotubes functionalized by H₂SO₄/HNO₃ oxidation. *Appl Surf Sci* 257:2401
- Khani H, Moradi O (2013) Influence of surface oxidation on the morphological and crystallographic structure of multi-walled carbon nanotubes via different oxidants. *J Nanostructure Chem* 3:73
- Paradise M, Goswami T (2007) Carbon nanotubes—production and industrial applications. *Mater Des* 28:1477
- Singh DK, Iyer PK, Giri PK (2010) Diameter dependence of interwall separation and strain in multiwalled carbon nanotubes probed by X-ray diffraction and Raman scattering studies. *Diamond Relat Mater* 19:1281
- Emmenegger C, Bonard J-M, Mauron P, Sudan P, Lepora A, Grobety B, Züttel A, Schlappach L (2003) Synthesis of carbon nanotubes over Fe catalyst on aluminium and suggested growth mechanism. *Carbon* 41:539
- Wirth CT, Bayer BC, Gamalski AD, Esconjauregui S, Weatherup RS, Ducati C, Baetz C, Robertson J, Hofmann S (2012) The

- phase of iron catalyst nanoparticles during carbon nanotube growth. *Chem Mater* 24:4633
38. Hiura H, Ebbesen T, Tanigaki K, Takahashi H (1993) Raman studies of carbon nanotubes. *Chem Phys Lett* 202:509
 39. Wepasnick KA, Smith BA, Bitter JL, Fairbrother DH (2010) Chemical and structural characterization of carbon nanotube surfaces. *Anal Bioanal Chem* 396:1003
 40. Liu Y, Pan C, Wang J (2004) Raman spectra of carbon nanotubes and nanofibers prepared by ethanol flames. *J Mater Sci* 39:1091. doi:10.1023/B:JMISC.0000012952.20840.09
 41. Sharifi T, Nitze F, Barzegar HR, Tai C-W, Mazurkiewicz M, Malolepszy A, Stobinski L, Wågberg T (2012) Nitrogen doped multi walled carbon nanotubes produced by CVD-correlating XPS and Raman spectroscopy for the study of nitrogen inclusion. *Carbon* 50:3535
 42. Hussain S, Amade R, Jover E, Bertran E (2013) Nitrogen plasma functionalization of carbon nanotubes for supercapacitor applications. *J Mater Sci* 48:7620. doi:10.1007/s10853-013-7579-z
 43. Jorio A, Pimenta MA, Filho AGS, Saito R, Dresselhaus G, Dresselhaus MS (2003) Characterizing carbon nanotube samples with resonance Raman scattering. *New J Phys* 5(139):131
 44. Saito R, Jorio A, Hafner JH, Lieber CM, Hunter M, McClure T, Dresselhaus G, Dresselhaus MS (2001) Chirality-dependent G-band Raman intensity of carbon nanotubes. *Phys Rev B* 64:085312
 45. Kim U-J, Furtado CA, Liu X, Chen G, Eklund PC (2005) Raman and IR spectroscopy of chemically processed single-walled carbon nanotubes. *J Am Chem Soc* 127:15437
 46. Chizari K, Vena A, Laurentius L, Sundararaj U (2014) The effect of temperature on the morphology and chemical surface properties of nitrogen-doped carbon nanotubes. *Carbon* 68:369
 47. Santangelo S, Lanza M, Milone C (2013) Evaluation of the overall crystalline quality of amorphous carbon containing multiwalled nanotubes. *J Phys Chem C* 117:4815
 48. Cao A, Xu C, Liang J, Wu D, Wei B (2001) X-ray diffraction characterization on the alignment degree of carbon nanotubes. *Chem Phys Lett* 344:13
 49. Zhang G, Mann D, Zhang L, Javey A, Li Y, Enilmez EY, Wang Q, McVittie JP, Nishi Y, Gibbons J, Dai H (2005) Ultra-high-yield growth of vertical single-walled carbon nanotubes: hidden roles of hydrogen and oxygen. *PNAS* 102:16141
 50. Dorris GM, Gray DG (1980) Adsorption of normal-alkanes at zero surface coverage on cellulose paper and wood fibers. *J Colloid Interface Sci* 77:353
 51. Menzel R, Lee A, Bismarck A, Shaffer MSP (2009) Inverse gas chromatography of as-received and modified carbon nanotubes. *Langmuir* 25:8340
 52. Khoo J, Burnett D, Menzel R, MSP Shaffer (2012) Surface energetic heterogeneity of carbon-based nanomaterials. www.TheSorptionSolution.com. Accessed 21 June 2012
 53. Vanyoreka L, Meszarosa R, Barany S (2014) Surface and electro-surface characterization of surface-oxidized multi-walled N-doped carbon nanotubes. *Colloids Surf A* 448:140
 54. Misra A, Tyagi PK, Singh MK, Misra DS (2006) FTIR studies of nitrogen doped carbon nanotubes. *Diamond Relat Mater* 15:385
 55. Maiyalagan T, Viswanathan B (2005) Template synthesis and characterization of well-aligned nitrogen containing carbon nanotubes. *Mater Chem Phys* 93:291
 56. Bandosz TJ (2009) Surface chemistry of carbon materials. In: Serp P, Fiueiredo JL (eds) *Carbon materials for catalysis*. Wiley, Hoboken, p 63
 57. Jianwei Z, Dazhi J, Hua-Xin P (2014) A pressurized filtration technique for fabricating carbon nanotube buckypaper: structure, mechanical and conductive properties. *Microporous Mesoporous Mater* 184:127
 58. Jianwei Z, Dazhi J, Hua-Xin P, Faxiang Q (2013) Enhanced mechanical and electrical properties of carbon nanotube buckypaper by in situ cross-linking. *Carbon* 63:125
 59. Latil S, Roche S, Mayou D, Charlier JC (2004) Mesoscopic transport in chemically doped carbon nanotubes. *Phys Rev Lett* 92(1):256805